HHS Public Access

Author manuscript

J Mater Chem B Mater Biol Med. Author manuscript; available in PMC 2015 December 10.

Published in final edited form as:

J Mater Chem B Mater Biol Med. 2015 October 1; 3(38): 7503–7510. doi:10.1039/C5TB01014D.

Silica-coated Gd(DOTA)-loaded protein nanoparticles enable magnetic resonance imaging of macrophages

Michael A. Bruckman[a,#], **Lauren N. Randolph**[a,#], **Neetu M. Gulati**[b], **Phoebe L. Stewart**[b], and **Nicole F. Steinmetz**[a,c,d,e,*]

[a]Department of Biomedical Engineering, Cleveland, OH

[b]Department of Pharmacology, Cleveland, OH

[c]Department of Radiology, Cleveland, OH

[d]Department of Materials Science and Engineering, Cleveland, OH

[e]Department of Macromolecular Science and Engineering Case Western Reserve University, Cleveland, OH

Abstract

The molecular imaging of *in vivo* targets allows non-invasive disease diagnosis. Nanoparticles offer a promising platform for molecular imaging because they can deliver large payloads of imaging reagents to the site of disease. Magnetic resonance imaging (MRI) is often preferred for clinical diagnosis because it uses non-ionizing radiation and offers both high spatial resolution and excellent penetration. We have explored the use of plant viruses as the basis of for MRI contrast reagents, specifically *Tobacco mosaic virus* (TMV), which can assemble to form either stiff rods or spheres. We loaded TMV particles with paramagnetic Gd ions, increasing the ionic relaxivity compared to free Gd ions. The loaded TMV particles were then coated with silica maintaining high relaxivities. Interestingly, we found that when Gd(DOTA) was loaded into the interior channel of TMV and the exterior was coated with silica, the T_1 relaxivities increased by three-fold from 10.9 mM^{-1} s^{-1} to 29.7 $mM^{-1}s^{-1}$ at 60 MHz compared to uncoated Gd-loaded TMV. To test the performance of the contrast agents in a biological setting, we focused on interactions with macrophages because the active or passive targeting of immune cells is a popular strategy to investigate the cellular components involved in disease progression associated with inflammation. *In vitro* assays and phantom MRI experiments indicate efficient targeting and imaging of macrophages, enhanced contrast-to-noise ratio was observed by shape-engineering (SNP > TMV) and silica-coating (Si-TMV/SNP > TMV/SNP). Because plant viruses are in the food chain, antibodies may be prevalent in the population. Therefore we investigated whether the silica-coating could prevent antibody recognition; indeed our data indicate that mineralization can be used as a stealth coating option to reduce clearance. Therefore, we conclude that the silica-coated protein-based contrast agent may provide an interesting candidate material for further investigation for *in vivo* delineation of disease through macrophage imaging.

*Corresponding author: nicole.steinmetz@case.edu.
#Authors contributed equally.

Introduction

Molecular imaging facilitates the early detection of disease, allows risk stratification, disease monitoring, longitudinal imaging and treatment follow up. A variety of imaging modalities have been developed, including positron electron tomography (PET), computed tomography (CT), and magnetic resonance imaging (MRI)(1). The latter is gaining popularity because of its excellent soft tissue contrast, spatial resolution and penetration depth, and because the non-ionizing radiation is safer for repeated imaging sessions. However, MRI has a low sensitivity to contrast-enhancement agents, which provide important information about molecular features *in vivo*(2). Nanoparticles are ideal platforms for the development of better contrast-enhancement agents because they can carry large payloads, they can be modified with targeting ligands to confer molecular specificity(3) and their structure enhances ionic relaxivity(4).

Several nanoparticle-based MRI contrast agents have been described, including nanoemulsions, dendrimers, silica and gold nanoparticles, and viral nanoparticles (VNPs) (4). Nanoparticles increase the longitudinal relaxivity (positive contrast, R_1) by reducing the molecular tumbling rate (τ_R) of chelated paramagnetic ions such as Gd following surface conjugation(5). In theory, free chelated Gd ions with a relaxivity of ~5 $mM^{-1}s^{-1}$ can achieve relaxivities of up to 80 mM^{-1} s^{-1} at 1.5 T, the common mode of MRI used in the clinic. This is based on the optimization of properties such as particle stiffness, bulk water accessibility and the chelating molecule, although experimentally it remains challenging to achieve such high values(5).

We have focused the development of VNPs for medical applications because the manufacture of such proteinaceous nanoparticles in a variety of shapes and sizes is highly reproducible and scalable, and the particles themselves are amenable to functionalization using synthetic biology, genetic engineering and bioconjugation chemistry(6). Several VNP-based MRI contrast agents have been described, including the icosahedral plant viruses *Cowpea mosaic virus* (CPMV)(7), *Cowpea chlorotic mottle virus* (CCMV)(8), bacteriophages P22(9), MS2(10) and Qβ(11), and the plant virus *Tobacco mosaic virus* (TMV), which naturally occurs as rods but can also be produced as spheres(12). A few recent articles discuss the *in vivo* performance of these protein-based MRI contrast agents(13–15). For example, we recently showed that TMV particles can be employed to image the molecular features of atherosclerotic plaques using a vascular cell adhesion molecule (VCAM-1)-targeted Gd(DOTA)-loaded probe(14). The T_1 relaxivity of this nanoparticle was ~15 mM^{-1} s^1yielding a per particle relaxivity of 35,000 mM^{-1} s^1 at 60 MHz, thus allowing the imaging of molecular features *in vivo* at submicromolar doses of Gd(DOTA).

In this work we set out to investigate the materials and biological properties of TMV-based MRI contrast agents, specifically we sought to develop probes for macrophage imaging. The active or passive targeting of immune cells is a popular strategy to investigate the cellular components involved in disease progression associated with inflammation. Macrophage imaging was studied as a function of contrast agent shape and surface coating. Protein-based nanoparticles (TMV rods and TMV spheres) were mineralized with silica coatings.

We chose silica as a coating material because it is biologically inert and coating techniques are well established(16). For example, silica mineralization has been used to improve the biocompatibility of nanoparticles based on gold(17), iron oxide(18) and quantum dots(19). We hypothesized that the silica coating would maintain high relaxivities, while providing a means for antibody evasion. Research indicates that TMV-specific antibodies are prevalent in the population due to presence of TMV in food and cigarettes(20, 21). Therefore, we investigated whether the silica shell would protect TMV and SNP from recognition by TMV-specific antibodies; this is an important goal for potential clinical application to prevent premature clearance of the contrast agent and maintain stable and reproducible pharmacokinetics for repeated imaging sessions.

In this article, we report i) the MRI properties of silica-coated vs. non-coated TMV rods and SNPs, ii) their applications for macrophage imaging as demonstrated by phantom MRI, and iii) the application of mineral coating as a method for antibody evasion.

Results and discussion

We based our nanoparticles on a mutant of TMV (S152K, TMVlys) that displays a reactive amine-functional lysine group at the solvent-exposed C-terminus of the coat protein(23). TMVlys was produced in *Nicotiana benthamiana* plants with a yield of 5 mg pure TMVlys particles per gram of infected leaf material. TMVlys comprises 2130 identical coat proteins arranged helically into a 300-nm soft-matter rod, 18 nm in diameter with a 4-nm internal channel. TMVlys was modified with paramagnetic Gd^{III} chelated to azido-mono amide-1,4,7,10-tetraazacyclododecane-*N*,*N*',*N*'',*N*'''-tetraacetic acid (DOTA-azide) to yield the MRI contrast-enhancement agent(12). The bioconjugation of Gd(DOTA) to the internal and external surfaces of TMVlys is described in detail in the Supporting Information and Figure S1. Briefly, terminal alkyne functionality was provided by modifying the tyrosine (TYR139) or glutamic acid (GLU 97/106) residues(24). Gd(DOTA) was attached to the terminal alkynes using a copper-catalyzed azide-alkyne cycloaddition reaction, forming internal Gd(DOTA) TMVlys (iGd-TMV) or external Gd(DOTA) TMVlys (eGd-TMV). TMVlys-based spherical nanoparticles (SNPs) were produced by heating iGd-TMV to 96°C for 60 s using a PCR thermocycler, forming Gd-SNP(12). Gd(DOTA) labeling efficiency (Figure 2A) was characterized by inductively-coupled plasma optical emission spectroscopy (ICP-OES) and matrix assisted laser desorption-ionization time-of-flight mass spectrometry (MALDI-TOF MS) as shown in Figure S2. TEM imaging was used to confirm the structural integrity of the TMV rods and spheres after chemical modification (Figure 1B). The TMV rods were modified with an average of 1000 Gd(DOTA) molecules per particle in both the internal and external labeling configurations. Similar loading density was achieved for SNPs, with 976 Gd(DOTA) per 2130 coat proteins (based on absorbance) on a particle with a diameter of ~75 nm and a density of 1.43 g/cm^3compared to 1.31 g/cm^3 for the TMV rods(25). This corresponds to an estimated 7074 coat proteins per sphere, yielding just over 3000 Gd(DOTA) labels per SNP.

Silica coatings were introduced as described(26) with modifications. Briefly, 1 ml tetraethyl orthosilicate (TEOS) as a 10% v/v stock in ethanol was mixed with 4 ml 5 M NH_4OH and 1 ml of modified TMVlys or SNPs (1 mg/ml in water) and diluted to 20 ml with ice-cold

ethanol. The reaction was allowed to proceed overnight (see Supporting Information). The resulting Si coat was ~65 nm deep, increasing the thickness of the nanoparticles to ~150 nm as shown by TEM and SEM (Figure 1B). The TMVlys mutant allowed the formation of a higher-quality silica coating compared to native TMV, because the positive charge of the solvent-exposed amine groups favored the nucleation of silica catalyzed by TEOS. The presence of silica was confirmed by TEM using electron dispersion spectroscopy (EDS) as shown in Figure S3. Silica mineralization presented the following challenges: First, the proportion of ethanol must be ~90% after all reactants have been added because lower concentrations increase the abundance of free silica particles, and high concentrations result in much thinner coatings. Additionally, salt must be removed from the TMV solution before mineralization. Sonication reduced aggregation and improved the dispersion of the mineralized particles. This is consistent with previous reports describing the silica mineralization of TMV(27–29), fd phage(30), and other nanoparticles(31). Silica is ideal as a coating material due to its biocompatibility, ease of surface functionalization, versatility, and stability(16, 32).

Next, we measured the longitudinal proton relaxivity of Gd(DOTA)-modified TMV rods and spheres (SNPs) using a standard inversion recovery sequence on a 60 MHz relaxometer (Bruker) at 37°C (Figure 2). Previously, we found that TMV externally modified with Gd(DOTA) had a higher ionic relaxivity than internally-modified particles due to increased stiffness of the tyrosine residue and better bulk water accessibility(12). Overall, we observed the same trend in the present study.

Throughout our investigation, we noted some batch-to-batch variations in the ionic relaxivity when we compared TMV samples with different Gd(DOTA) loading rates. Therefore, we set out to determine whether the Gd(DOTA) density affected the ionic relaxivity of the particles. TMV rods with Gd(DOTA) loads ranging from 429 to 1477 Gd per particle were prepared and the ionic relaxivities were determined (Figure S4). We found an inverse correlation between ionic relaxivity and Gd(DOTA) density. Although the per-particle relaxivity increased at higher Gd density, the ionic relaxivity decreased at higher Gd density. If the Gd(DOTA) ions are distributed in a statistically random manner, the lower-density formulation may offer greater inter-Gd(DOTA) spacing and therefore may increase the number of water molecules showing interactions at any given time. Others have shown that greater spacing between Gd ions (lower density) can increase overall relaxivity by increasing the transverse electronic relaxivity of the ions. Interactions between nearby paramagnetic centers increase the electronic relaxation of the electron spins of Gd ions, thereby reducing the water relaxivity(33). For example, micelles fully loaded (100%) with chelated Gd were able to achieve relaxivities of 30.0 mM^{-1} s^{-1} at 20 MHz, whereas micelles loaded with 98% Y and 2% Gd achieved a relaxivity of 41.4 $mM^{-1}s^{-1}$ at 20 MHz(34). Alternatively, if we consider iGd-TMV and assume the labeling density increases at the open ends, this would allow for more efficient water exchange with the bulk water surrounding the TMV rod without limiting water exchange in the 4-nm internal channel. Indeed, similar trends have been reported with mesoporous silica nanoparticles labeled with Gd when the entrance to the pores is compared to the entire structure(35).

Next, we compared the relaxivities of mineralized TMV rods and SNPs *versus* their native counterparts. The ionic and per particle relaxivities remained consistent for eGd-TMV (23.5 vs 24.8 mM^{-1} s^{-1}) and SNP (17.7 vs 16.5 mM^{-1} s^{-1}) following silica coating (Figure 2). Silica mineralization alone did not change the relaxivity compared to concentration-matched unlabeled TMVlys particles (Figure 2F). In stark contrast, a nearly three-fold increase in relaxivity was observed for mineralized *versus* native iGd-TMV particles, i.e. there was an increase from 10.9 to 29.7 mM^{-1} s^{-1} at 60 MHz which is presented as a bar chart (Figure 2B) and in the form of relaxivity curves (Figure 2C-F).

Two factors may promote this increased relaxivity. First, mineralization around the TMV scaffold creates a dense surface coating that may trap bulk water inside the 4-nm channel resulting in differential water flux connecting the bulk surrounding water and the bulk internal water, maintaining and increasing the molecular interactions between Gd molecules and internal bulk water, therefore increasing the relaxivity of iGd-TMV but not eGd-TMV. Given that the silica-coated eGd-TMV and Gd-SNP formulations exhibited T_1 values comparable to their native forms suggests that mesoporous silica is formed enabling water exchange through the silica coat. High-resolution TEM confirms the formation of mesoporous silica shells on the TMV rods and spheres (Figure S5). Second, particle stiffness increases when the silica coating is applied, and this may increase the relaxivity by inhibiting the molecular tumbling of Gd(DOTA). Nanoparticle rigidity can be calculated using the Lipari-Szabo approach, which identifies an order parameter for the local and global rotations with limiting values $0 < S^2 < 1$, where 1 is a completely rigid nanoparticle and 0 is a fully independent contrast agent(2). Stiffer nanoparticles have higher order parameter values (S^2) and therefore yield a higher ionic relaxivity(36).

To test the performance of the contrast agents in a biological setting, we focused on interactions with macrophages because the active or passive targeting of immune cells is a popular strategy to investigate the cellular components involved in disease progression. For example, targeting macrophages in cardiovascular disease can provide insight into the composition of atherosclerotic plaques and may facilitate risk stratification. A macrophage-rich and lipid-rich plaque with a thin fibrous cap may indicate a plaque vulnerable to rupture(37–40). We therefore used RAW 264.7 murine macrophages as a model system(41, 42). We tested the uptake of TMV rods and spheres before and after mineralization by flow cytometry using fluorescence-labeled particles (Figures 3A and 3B) and then tested the Gd(DOTA)-labeled formulations in MRI experiments (Figure 3C and 3D). The labeling strategy and characterization of fluorescent particles is described in the Supporting Information.

Time-course flow cytometry showed that the silica coating significantly increased the number of interactions between macrophages and the TMV nanoparticles, regardless of their shape (Figure 3A, see Supporting Information for detailed methods) agreeing with previous reports showing that macrophages rapidly scavenge silica nanoparticles(43, 44). The non-coated SNPs were much more readily taken up by the macrophages than TMVlys rods (Figure 3A). This is consistent with our recent study showing that macrophages interact more efficiently with TMV particles with a low aspect ratio(45). The high aspect ratio of the elongated stiff rod promotes immune evasion by inhibiting phagocytosis. This is a well-

known phenomenon in nanomedicine and can be advantageous if cellular or molecular components other than macrophages are the desired target(46).

We next investigated whether the Gd-labeled TMV and SNP formulations could be used to detect macrophages in a pre-clinical MRI scanner (Figure 3C, see Supporting Information for detailed methods). Briefly, cells were incubated with the different MRI contrast agents and controls, and were then pelleted by centrifugation and analyzed using a 7.0T (300 MHz) MRI (Bruker BioSpec 70/30USR). Following multiple scouting scans, a T_1-weighted Multi Slice Multi Echo (MSME) sequence was used with the following parameters: TR/TE = 600/8.0 ms, 1 mm thickness, four averages, matrix = 128×128, field of view = 2.98 cm. Exported DICOM images were analyzed with the free open software OsiriX.

Macrophages were quantified by measuring the contrast-to-noise ratio (CNR) of cell pellets compared to the buffer solution for each well. We found that silica-coated TMV rods and SNPs showed higher CNRs than their non-mineralized counterparts (Figure 3D), which is consistent with the interactions observed by flow cytometry (Figure 3B). Additionally, SNPs yielded higher CNRs than TMV rods confirming that SNPs target macrophages more efficiently than rods. The experiments were reproducible over a range of cell and particle concentrations (Figure S6).

Together, these results demonstrate that SNP, Si-TMV and Si-SNP particles are suitable for the imaging of macrophage-rich diseases. We have previously shown that targeted rod-shaped TMV particles are appropriate for MRI applied to vasculature molecular markers in atherosclerotic plaques(14). TMV rods could therefore be combined with SNPs to image molecular markers and macrophages, providing a powerful tool to facilitate risk stratification and the prognosis of atherosclerosis patients.

Lastly, we set out to determine whether the silica coating would protect the TMV protein-based contrast agents from antibody recognition. VNPs, much like other protein-based nanoparticles, are prone to elicit the production of VNP-specific antibodies when introduced as ‘naked’ versions into the body. Furthermore, early research has shown that TMV-specific antibodies are prevalent due to presence of TMV in food and cigarettes(20, 21). Therefore, we investigated whether the silica shell would protect TMV (and SNP) from recognition by the immune system. This is an important requirement in translational applications because antibody binding can interfere with target recognition and alter the fate of nanoparticle-based MRI contrast-enhancing reagents, particularly if repeat administration is necessary.

To determine the ability of the thick silica coating to prevent antibody recognition, immunogold staining experiments were carried out in which TMV, SNP, Si-TMV or Si-SNP were deposited on TEM grids followed by the application of TMV-specific antibodies and detection using 10-nm gold immunoconjugate secondary antibodies (Figure 4, see Supporting Information for details). Accordingly, we found that the non-coated SNP and TMV particles were efficiently recognized by the antibodies, whereas the silica-coated TMV and SNP formulations were shielded from antibody recognition. This was confirmed by testing mixed preparations of TMV and Si-TMV, which resulted in the specific recognition of the non-coated TMV particles (Figure 4E). Silica coatings could therefore be applied as

an alternative to polyethylene glycol (PEG) shielding to avoid antibody recognition. We have previously shown that PEG shielding yields stealth VNPs that are not recognized by antibodies(47). Whereas Si is known to improve the biocompatibility and reduce the toxicity nanoparticles based on gold(17), iron oxide(18) and quantum dots(19), this is the first demonstration that Si can also circumvent immune surveillance.

Conclusion

We synthesized rod-shaped and spherical silica-coated TMV nanoparticles loaded with Gd(DOTA). Silica-coated contrast agents maintained high relaxivities, therefore providing a potential candidate material for MRI applications. Interestingly, we found that the mineralization of TMV rods labeled internally with Gd(DOTA) increased the ionic relaxivity of the particles three-fold compared to non-mineralized particles, potentially reflecting the increased particle stiffness. Medical relevance was determined *in vitro* using the murine macrophage cell line RAW 264.7. These studies serve as a proof-of-concept; detection and imaging of macrophages may aid diagnosis and prognosis of disease associated with inflammation, such as cardiovascular diseases. Imaging studies demonstrate increased macrophage targeting as a function of nanoparticle shape and surface coating with SNP>TMV and Si-coated SNP/TMV>native SNP/TMV. Lastly, we demonstrate that the silica-coating effectively reduced antibody binding, which is important for the translational development of these MRI contrast agents. This versatile mineralization protocol could also be applied to other platforms for biological macromolecule cargo delivery to reduce immunogenicity and may improve MRI contrast relaxivity.

Supplementary Material

Refer to Web version on PubMed Central for supplementary material.

Acknowledgments

This work was supported in part by grants from the National Science Foundation (CMMI NM 1333651 to NFS) and National Institutes of Health (NIH R21HL121130 to NSF). MAB acknowledges the NIH T32 HL105338 Cardiovascular Research Institute training grant. NMG acknowledges the NIH T32 GM008803 Molecular Therapeutics training grant.

References

1. Mulder WJM, Jaffer FA, Fayad ZA, Nahrendorf M. Imaging and nanomedicine in inflammatory atherosclerosis. Science Translational Medicine. 2014; 6(239):239sr1. [PubMed: 24898749]
2. Verwilst P, Park S, Yoon B, Kim JS. Recent advances in Gd-chelate based bimodal optical/MRI contrast agents. Chemical Society Reviews. 2015; 44(7):1791–1806. [PubMed: 25622561]
3. Zhang L, Gu FX, Chan JM, Wang AZ, Langer RS, Farokhzad OC. Nanoparticles in Medicine: Therapeutic Applications and Developments. Clinical Pharmacology and Therapeutics. 2007; 83(5): 761–769. [PubMed: 17957183]
4. Bruckman MA, Yu X, Steinmetz NF. Engineering Gd-loaded nanoparticles to enhance MRI sensitivity via T1shortening. Nanotechnology. 2013; 24(46):462001. [PubMed: 24158750]
5. Caravan P, Farrar CT, Frullano L, Uppal R. Influence of molecular parameters and increasing magnetic field strength on relaxivity of gadolinium- and manganese-based T 1contrast agents. 2009; 4(2):89–100.

6. van Kan-Davelaar HE, van Hest J, Cornelissen J, Koay M. Using viruses as nanomedicines. British Journal of Pharmacology. 2014; 171(17):4001–4009. [PubMed: 24571489]
7. Prasuhn DE, Yeh RM, Obenaus A, Manchester M, Finn MG. Viral MRI contrast agents: coordination of Gd by native virions and attachment of Gd complexes by azide?alkyne cycloaddition. Chemical Communications. 2007; (12):1269. [PubMed: 17356779]
8. Liepold L, Anderson S, Willits D, Oltrogge L, Frank JA, Douglas T, et al. Viral capsids as MRI contrast agents. Magnetic Resonance in Medicine. 2007; 58(5):871–879. [PubMed: 17969126]
9. Qazi S, Liepold LO, Abedin MJ, Johnson B, Prevelige P, Frank JA, et al. P22 Viral Capsids as Nanocomposite High-Relaxivity MRI Contrast Agents. Molecular Pharmaceutics. 2012; 10(1):11–17. [PubMed: 22656692]
10. Garimella PD, Datta A, Romanini DW, Raymond KN, Francis MB. Multivalent, High-Relaxivity MRI Contrast Agents Using Rigid Cysteine-Reactive Gadolinium Complexes. Journal of the American Chemical Society. 2011; 133(37):14704–14709. [PubMed: 21800868]
11. Pokorski JK, Breitenkamp K, Liepold LO, Qazi S, Finn MG. Functional Virus-Based Polymer–Protein Nanoparticles by Atom Transfer Radical Polymerization. Journal of the American Chemical Society. 2011; 133(24):9242–9245. [PubMed: 21627118]
12. Bruckman MA, Hern S, Jiang K, Flask CA, Yu X, Steinmetz NF. Tobacco mosaic virus rods and spheres as supramolecular high-relaxivity MRI contrast agents. Journal of Materials Chemistry B. 2013; 1(10):1482.
13. Min J, Jung H, Shin H-H, Cho G, Cho H, Kang S. Implementation of P22 Viral Capsids As Intravascular Magnetic Resonance T1Contrast Conjugates via Site-Selective Attachment of Gd(III)-Chelating Agents. Biomacromolecules. 2013; 14(7):2332–2339. [PubMed: 23758486]
14. Bruckman MA, Jiang K, Simpson EJ, Randolph LN, Luyt LG, Yu X, et al. Dual-Modal Magnetic Resonance and Fluorescence Imaging of Atherosclerotic Plaques in Vivo Using VCAM-1 Targeted Tobacco Mosaic Virus. Nano Letters. 2014; 14(3):1551–1558. [PubMed: 24499194]
15. Shukla S, Steinmetz NF. Virus-based nanomaterials as positron emission tomography and magnetic resonance contrast agents: from technology development to translational medicine. Wiley interdisciplinary reviews Nanomedicine and nanobiotechnology. 2015 early view.
16. Tarn D, Ashley CE, Xue M, Carnes EC, Zink JI, Brinker CJ. Mesoporous Silica Nanoparticle Nanocarriers: Biofunctionality and Biocompatibility. Accounts of Chemical Research. 2013; 46(3):792–801. [PubMed: 23387478]
17. Lee JY, Park W, Yi DK. Immunostimulatory effects of gold nanorod and silica-coated gold nanorod on RAW 264.7 mouse macrophages. Toxicology Letters. 2012; 209(1):51–57. [PubMed: 22155353]
18. Singh RK, Kim T-H, Patel KD, Knowles JC, Kim H-W. Biocompatible magnetite nanoparticles with varying silica-coating layer for use in biomedicine: Physicochemical and magnetic properties, and cellular compatibility. Journal of Biomedical Materials Research Part A. 2012; 100A(7):1734–1742. [PubMed: 22447364]
19. Durgadas CV, Sreenivasan K, Sharma CP. Bright blue emitting CuSe/ZnS/silica core/shell/shell quantum dots and their biocompatibility. Biomaterials. 2012; 33(27):6420–6429. [PubMed: 22704598]
20. Balique F, Colson P, Barry AO, Nappez C, Ferretti A, Moussawi KA, et al. Tobacco Mosaic Virus in the Lungs of Mice following Intra-Tracheal Inoculation. PLoS ONE. 2013; 8(1):e54993. [PubMed: 23383021]
21. Liu R, Vaishnav RA, Roberts AM, Friedland RP. Humans Have Antibodies against a Plant Virus: Evidence from Tobacco Mosaic Virus. PLoS ONE. 2013; 8(4):e60621. [PubMed: 23573274]
22. Carniato F, Tei L, Cossi M, Marchese L, Botta M. A Chemical Strategy for the Relaxivity Enhancement of GdIII Chelates Anchored on Mesoporous Silica Nanoparticles. Chemistry - A European Journal. 2010; 16(35):10727–10734.
23. Geiger FC, Eber FJ, Eiben S, Mueller A, Jeske H, Spatz JP, et al. TMV nanorods with programmed longitudinal domains of differently addressable coat proteins. Nanoscale. 2013; 5(9):3808–3816. [PubMed: 23519401]

24. Bruckman MA, VanMeter A, Steinmetz NF. Nanomanufacturing of Tobacco Mosaic Virus-Based Spherical Biomaterials Using a Continuous Flow Method. ACS Biomaterials Science & Engineering. 2015; 1(1):13–18. [PubMed: 25984569]
25. Dobrov EN, Nikitin NA, Trifonova EA, Parshina EY, Makarov VV, Maksimov GV, et al. β-structure of the coat protein subunits in spherical particles generated by tobacco mosaic virus thermal denaturation. Journal of Biomolecular Structure and Dynamics. 2014; 32(5):701–708. [PubMed: 24404770]
26. Stober W, Fink A, Bohn E. Controlled Growth of Monodisperse Silica Spheres in Micron Size Range. Journal of Colloid and Interface Science. 1968; 26(1):62–69.
27. Royston E, Lee S-Y, Culver JN, Harris MT. Characterization of silica-coated tobacco mosaic virus. Journal of Colloid and Interface Science. 2006; 298(2):706–712. [PubMed: 16426631]
28. Royston ES, Brown AD, Harris MT, Culver JN. Preparation of silica stabilized Tobacco mosaic virus templates for the production of metal and layered nanoparticles. Journal of Colloid and Interface Science. 2009; 332(2):402–407. [PubMed: 19159894]
29. Fowler CE, Shenton W, Stubbs G, Mann S. Tobacco Mosaic Virus Liquid Crystals as Templates for the Interior Design of Silica Mesophases and Nanoparticles. Advanced Materials. 2001; 13(16):1266–1269.
30. Zhang Z, Buitenhuis J. Synthesis of Uniform Silica Rods, Curved Silica Wires, and Silica Bundles Using Filamentousfd Virus as a Template. Small. 2007; 3(3):424–428. [PubMed: 17262866]
31. Liu B, Cao Y, Huang Z, Duan Y, Che S. Silica Biomineralization via the Self-Assembly of Helical Biomolecules. Advanced Materials. 2014; 27(3):479–497. [PubMed: 25339438]
32. Tamba BI, Dondas A, Leon M, Neagu AN, Dodi G, Stefanescu C, et al. Silica nanoparticles: Preparation, characterization and in vitro/in vivo biodistribution studies. European Journal of Pharmaceutical Sciences. 2015; 71:46–55. [PubMed: 25681629]
33. Nicolle, GlM; Helm, L.; Merbach, AE. 8S paramagnetic centres in molecular assemblies: possible effect of their proximity on the water proton relaxivity. Magnetic Resonance in Chemistry. 2003; 41(10):794–799.
34. Gianolio E, Giovenzana GB, Longo D, Longo I, Menegotto I, Aime S. Relaxometric and Modelling Studies of the Binding of a Lipophilic Gd-AAZTA Complex to Fatted and Defatted Human Serum Albumin. Chemistry - A European Journal. 2007; 13(20):5785–5797.
35. Davis JJ, Huang W-Y, Davies G-L. Location-tuned relaxivity in Gd-doped mesoporous silica nanoparticles. Journal of Materials Chemistry. 2012; 22(43):22848–22850. [PubMed: 26052183]
36. Botta M, Tei L. Relaxivity Enhancement in Macromolecular and Nanosized GdIII-Based MRI Contrast Agents. European Journal of Inorganic Chemistry. 2012; 2012(12):1945–1960.
37. Trivedi R, J UK-I, Gillard J. Accumulation of ultrasmall superparamagnetic particles of iron oxide in human atherosclerotic plaque. Circulation. 2003; 108(19):e140. [PubMed: 14610003]
38. Kooi ME, Cappendijk VC, Cleutjens KB, Kessels AG, Kitslaar PJ, Borgers M, et al. Accumulation of ultrasmall superparamagnetic particles of iron oxide in human atherosclerotic plaques can be detected by in vivo magnetic resonance imaging. Circulation. 2003; 107(19):2453–2458. [PubMed: 12719280]
39. Tang T, Howarth SP, Miller SR, Trivedi R, Graves MJ, King-Im JU, et al. Assessment of inflammatory burden contralateral to the symptomatic carotid stenosis using high-resolution ultrasmall, superparamagnetic iron oxide-enhanced MRI. Stroke. 2006; 37(9):2266–2270. [PubMed: 16917091]
40. Tang TY, Muller KH, Graves MJ, Li ZY, Walsh SR, Young V, et al. Iron oxide particles for atheroma imaging. Arterioscler Thromb Vasc Biol. 2009; 29(7):1001–1008. [PubMed: 19229073]
41. Dobrovolskaia MA, Aggarwal P, Hall JB, McNeil SE. Preclinical Studies To Understand Nanoparticle Interaction with the Immune System and Its Potential Effects on Nanoparticle Biodistribution. Molecular Pharmaceutics. 2008; 5(4):487–495. [PubMed: 18510338]
42. Nel AE, Mädler L, Velegol D, Xia T, Hoek EMV, Somasundaran P, et al. Understanding biophysicochemical interactions at the nano–bio interface. Nature Materials. 2009; 8(7):543–557. [PubMed: 19525947]

43. Zhu X-M, Fang C, Jia H, Huang Y, Cheng CH, Ko C-H, et al. Cellular uptake behaviour, photothermal therapy performance, and cytotoxicity of gold nanorods with various coatings. Nanoscale. 2014; 6(19):11462–11472. [PubMed: 25155843]

44. Yu T, Malugin A, Ghandehari H. Impact of Silica Nanoparticle Design on Cellular Toxicity and Hemolytic Activity. ACS Nano. 2011; 5(7):5717–5728. [PubMed: 21630682]

45. Shukla S, Eber FJ, Nagarajan AS, DiFranco NA, Schmidt N, Wen AM, et al. The Impact of Aspect Ratio on the Biodistribution and Tumor Homing of Rigid Soft-Matter Nanorods. Adv Healthc Mater. 2015; 4(6):874–882. [PubMed: 25641794]

46. Wen AM, Rambhia PH, French RH, Steinmetz NF. Design rules for nanomedical engineering: from physical virology to the applications of virus-based materials in medicine. Journal of Biological Physics. 2013; 39(2):301–325. [PubMed: 23860875]

47. Lee KL, Shukla S, Wu M, Ayat NR, El Sanadi CE, Wen AM, et al. Stealth filaments: Polymer chain length and conformation affect the in vivo fate of PEGylated potato virus X. Acta Biomater. 2015; 19:166–179. [PubMed: 25769228]

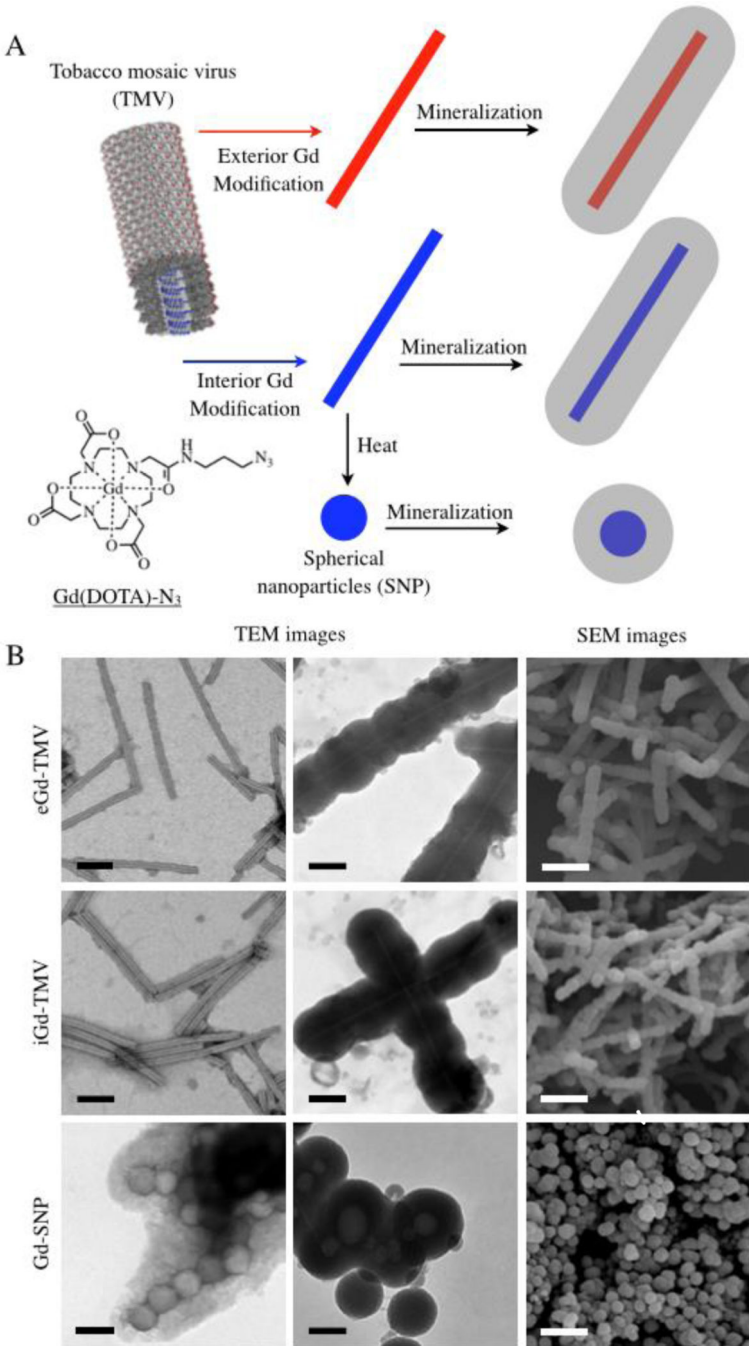

Figure 1.

A) The bioconjugation and mineralization scheme which produces Gd(DOTA)-loaded and silica-coated TMV rods and spheres. **B**) TEM and SEM imaging of TMV-based contrast agents. Scale bars = 100 nm (TEM, black) or 500 nm (SEM, white).

A

Sample	Gd per Particle	Relaxivity per Gd	Relaxivity per Particle
Gd(DOTA)	1	5	5
iGd-TMV	1,061	10.9	11,555
iGd-TMV-Si	1,061	29.7	31,537
eGd-TMV	1,090	23.5	25,587
eGd-TMV-Si	1,090	24.8	26,979
Gd-SNP	3,018*	17.7	53,513
Gd-SNP-Si	3,018*	16.5	49,717

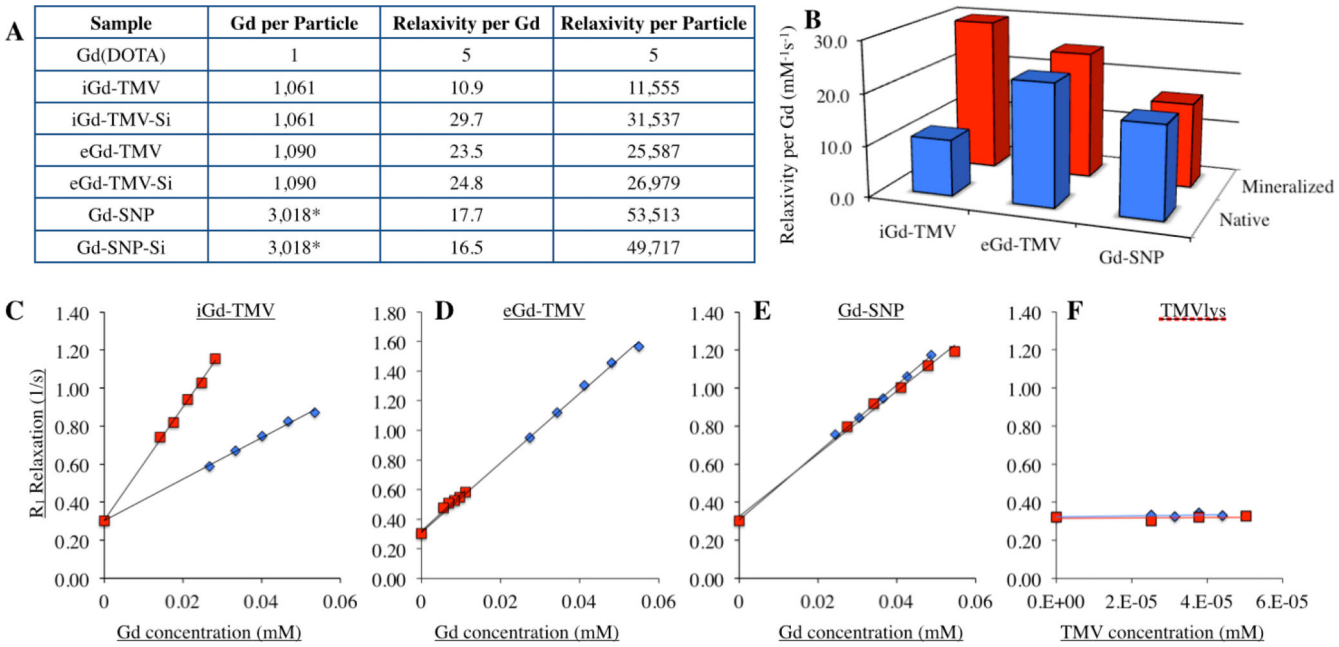

Figure 2.

(**A**) Table and accompanying (**B**) bar graph showing Gd loading per particle, relaxivity per Gd and per particle (in mM^{-1} s^{-1} at 60 MHz). The lower panels show relaxivity curves for (**C**) iGd-TMV, (**D**) eGd-TMV, (**E**) Gd-SNP, and (**F**) unmodified TMV. Blue curves are pre-mineralized (native) particles and red curves are post-mineralized particles. TMVlys shows the relaxivity curves for unlabeled TMVlys at virus concentrations matching values for iGd-TMV curves. *Gd per SNP calculated based on their size/volume relationships.

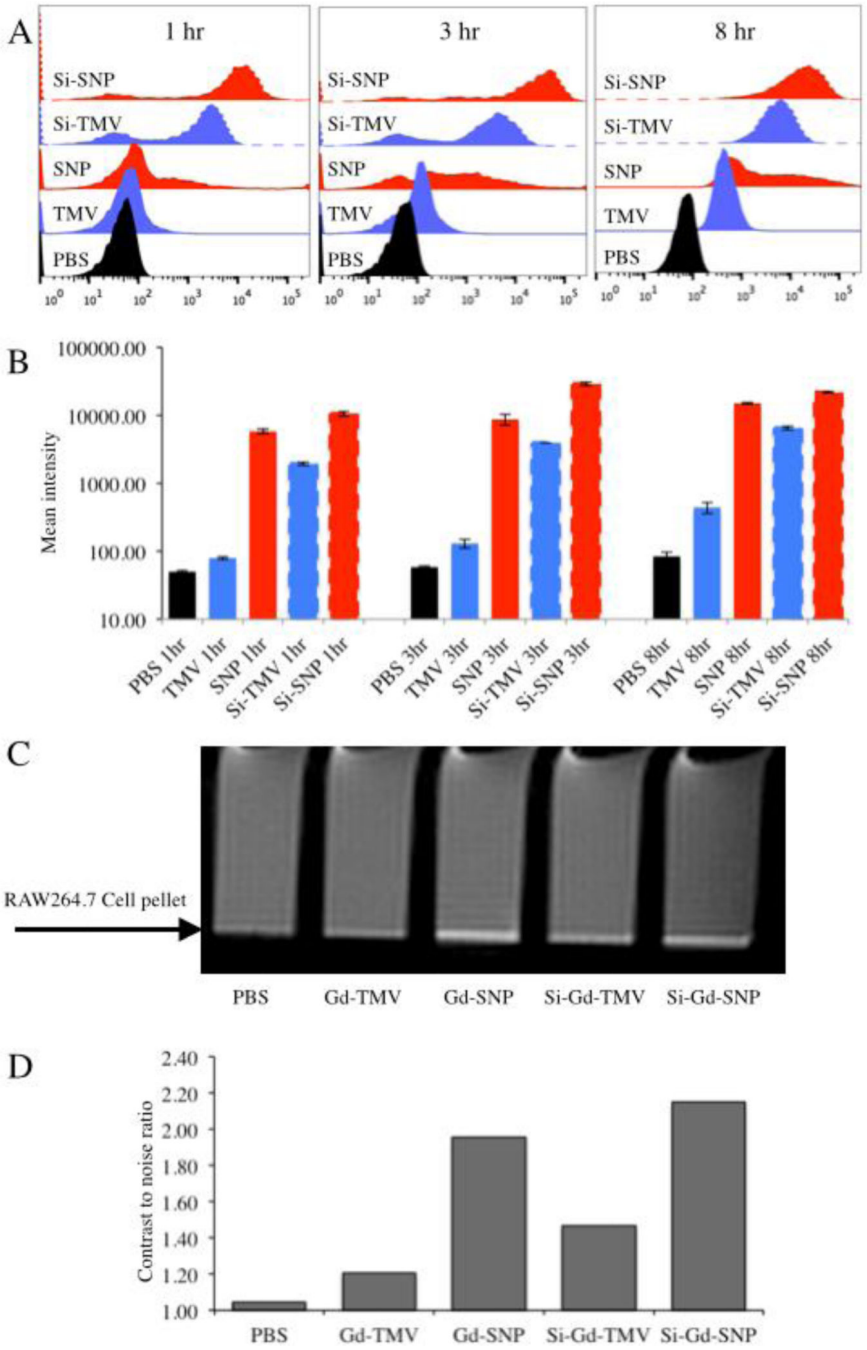

Figure 3.

(**A**) Histograms from flow cytometry studies showing TMV, SNP, Si-TMV and Si-SNP interactions with RAW 264.7 cells 1, 3, and 8 h after exposure using fluorescent TMV and SNP formulations. (**B**) Mean intensity plotted versus time and per particle formulation as a quantitative measure of cell interactions. (**C**) MRI phantom images of RAW 264.7 cell pellets 8 h after binding with TMV, SNP, Si-TMV and Si-SNP. Gd(DOTA)-labeled TMV and SNP formulations were incubated with RAW 264.7 cells for 8 h, then cells were washed and pelleted prior to obtaining MRI images using a 7.0T (300 MHz) MRI (Bruker BioSpec

70/30USR). The arrow indicates the cell pellets, a positive signal shows as bright pixels. (D) Cell interactions were quantified by contrast-to-noise (CNR) ratio of the MRI phantom image (cell pellets vs. medium).

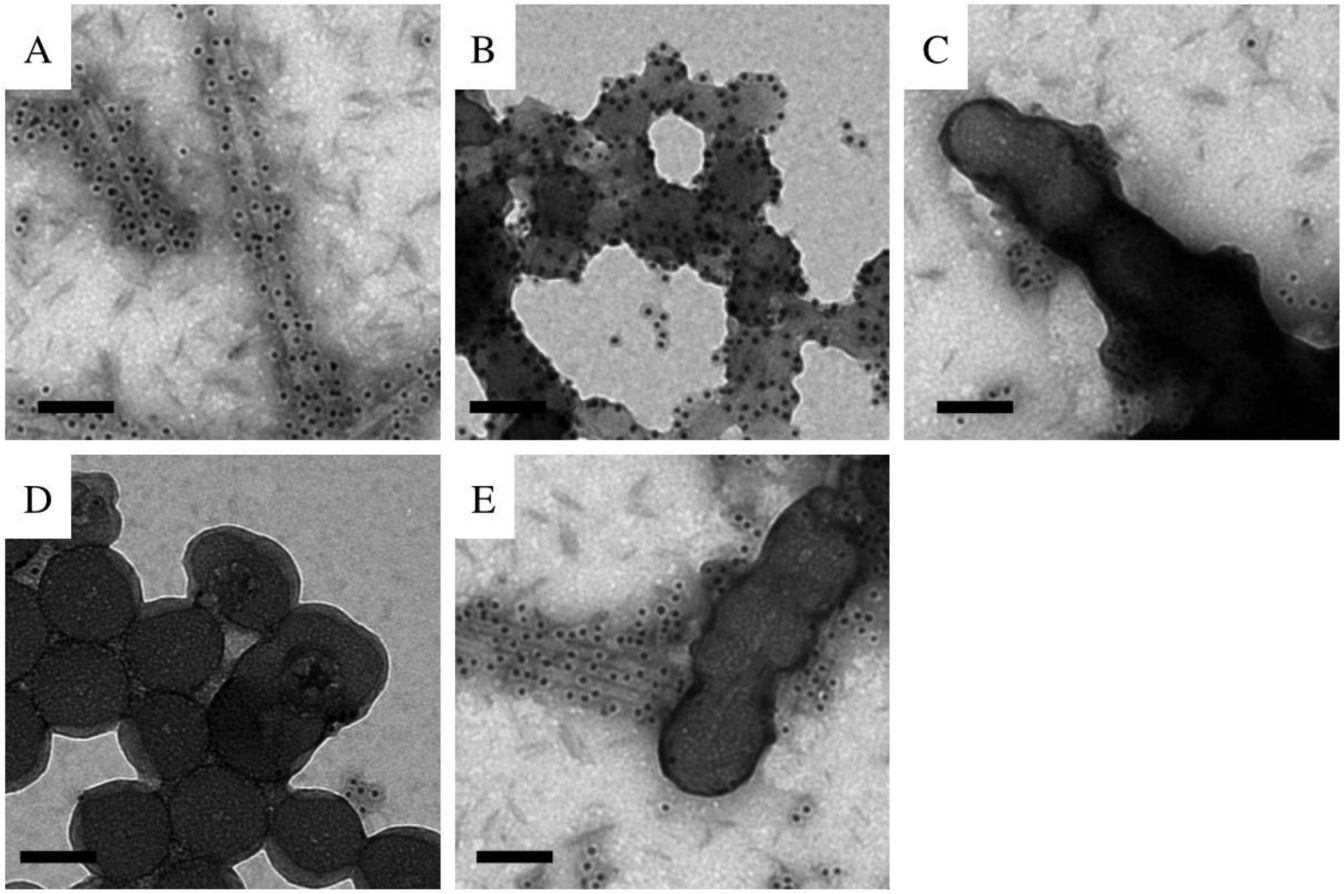

Figure 4.
Binding of gold-labeled anti-TMV antibodies to (A) TMV, (B) SNP, (C) Si-TMV, (D) Si-SNP, and (E) a mix of TMV and Si-TMV. Scale bars = 100 nm.